Supplementary Information

Unraveling the effects of geometrical parameters on dynamic impact responses of graphene reinforced polymer nanocomposites using coarse-grained molecular dynamics simulations

Jianzheng Cui[1], Fanlin Zeng[1], *, Dahai Wei[1], Youshan Wang[2]

[1]Department of Astronautic Science and Mechanics, Harbin Institute of Technology, Harbin, People's Republic of China

[2]National Key Laboratory of Science and Technology on Advanced Composites in Special Environment, Center for Composite Materials, Harbin Institute of Technology, Harbin, People's Republic of China

S1. Snapshots of AA and CG models during the pull-out of graphene.

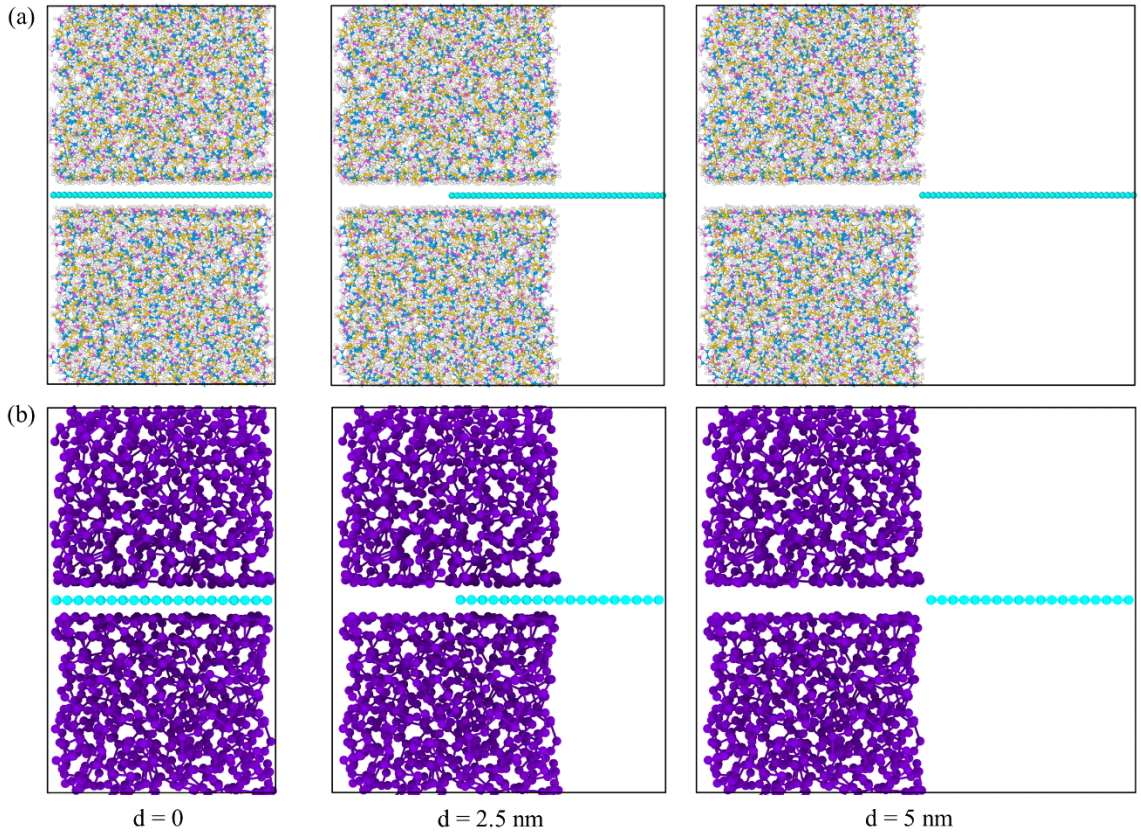

Fig. S1. Snapshots of (a) AA and (b) CG models during the pull-out of graphene.

S2. Verification of the interfacial CG force field between NR and graphene.

To verify that the interfacial CG force field between NR and graphene obtained in this work can accurately predict the density and structural properties at the interface, a periodic NR/graphene interface model with a size of 5 × 5 × 8 nm^3 is constructed, and the mass density profile along the *z* direction is calculated and shown in Fig. S2. From Fig. S2(c), the density profiles of NR chains in the two interface models reach a peak at NR/graphene interface, which can be attributed to the physical adsorption of NR chains on the surface of graphene [S1]. It is worth noting that a larger density oscillation amplitude (higher peaks and lower valleys) and period can be observed at the interface in the CG model compared to the AA model, which can be attributed to reduced surface roughness of graphene caused by the 4:1 CG modeling. This phenomenon also emphasizes the importance of selecting the appropriate degree of coarse-graining of graphene for the study of interface behavior of the nanocomposites. Meanwhile, the average mass densities of NR chains in the AA and CG interface models are obtained to be 0.95 and 0.96 g/cm^3, which verifies that our CG model can accurately reproduce and predict the interfacial structural properties of NR/graphene

nanocomposites.

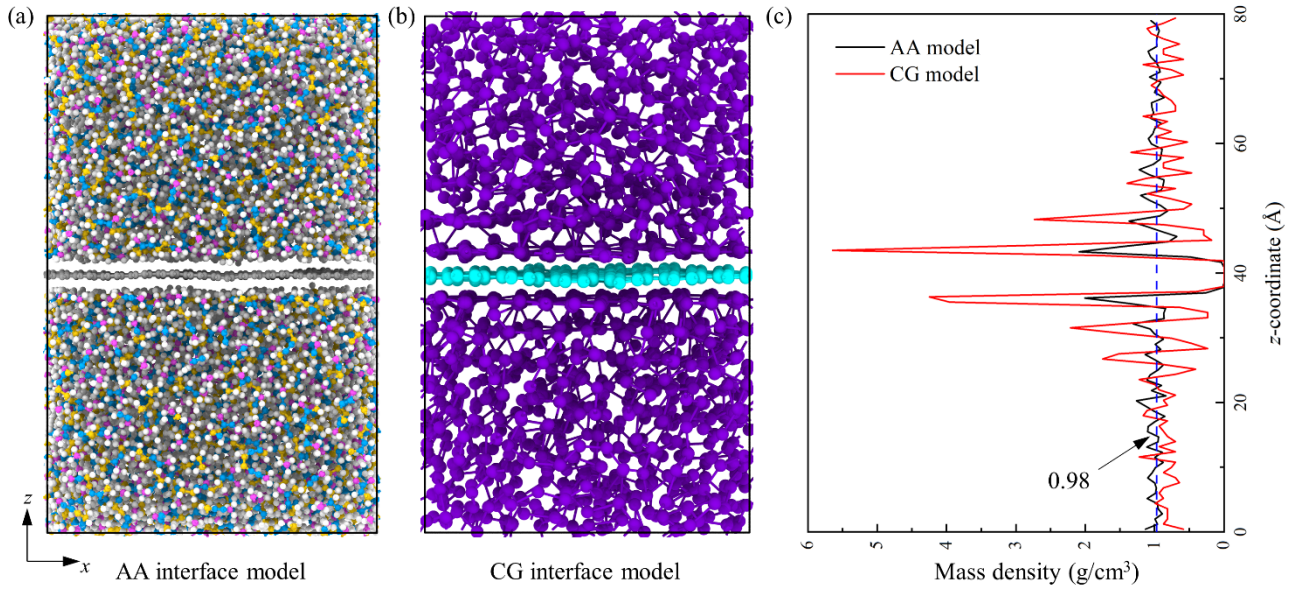

Fig. S2. Molecular configurations of (a) AA and (b) CG interface models, (c) mass density profile of NR molecular chains along the *z* direction.

S3. Selection of cut-off distance.

Fig. S3 shows the variations of the non-bond vdW energy between components with pair distance, which indicates that when the cut-off distances for vdW interactions for NR-NR, graphene-graphene, and NR-graphene are 25, 12, and 18 Å, respectively, the corresponding non-bond vdW energy tends to zero. Combining computational efficiency and accuracy, the cut-off distances for vdW interactions for NR-NR, graphene-graphene, and NR-graphene are hence set to 25, 12, and 18 Å, respectively.

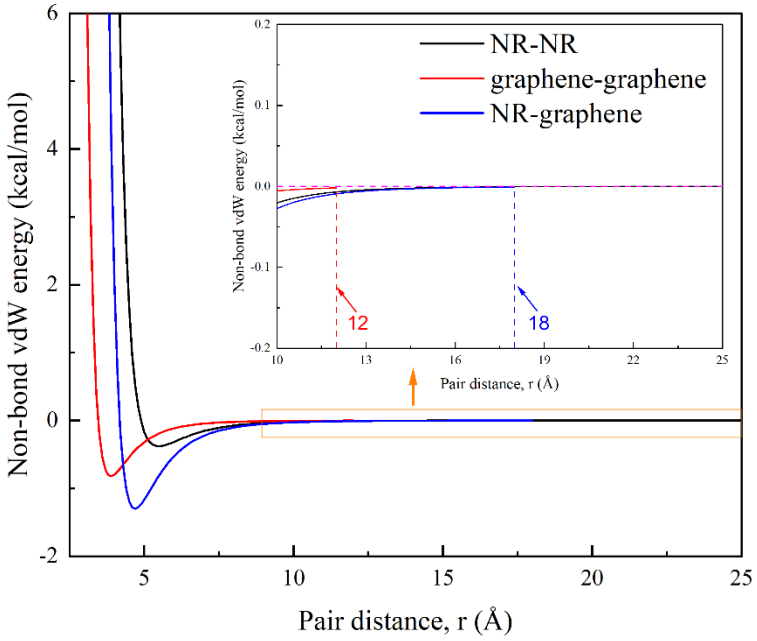

Fig. S3. Non-bond vdW energy curves between components in the nanocomposites.

S4. Verification of equilibrium state.

We take the system with 4 nm interlayer distance as an example to verify that all our systems are sufficiently well equilibrated before calculating the dynamic impact responses. Thermodynamically, the system's density and total energy have stabilized during equilibrium, as shown in Fig. S4(a). Structurally, the root-mean-square (RMS) end-to-end distance and RMS radius of gyration of NR molecular chains are already in dynamic equilibrium, as shown in Fig. S4(b). Dynamically, the mean square displacement (MSD) of NR molecular chains tends to stabilize, and the diffusion coefficient is only 0.018 $Å^2$/ps, as plotted in Fig. S4(c). These results indicate that the nanocomposite system is adequately equilibrated before calculating the mechanical properties by combining thermodynamic and structural analysis.

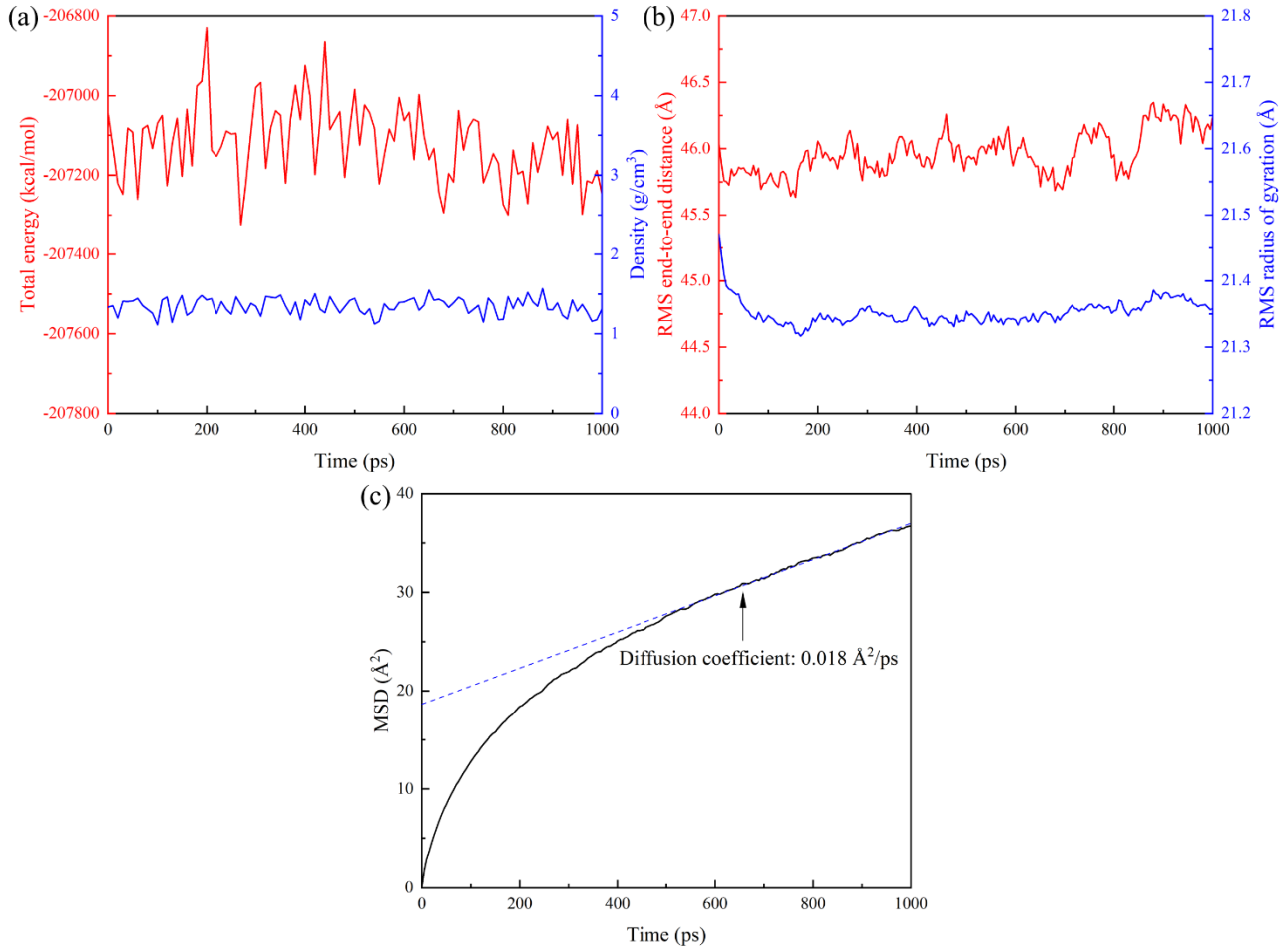

Fig. S4. Variations of (a) total energy and density of the nanocomposites, (b) RMS end-to-end distance and RMS radius of gyration of NR molecular chains, (c) MSD as well as diffusion coefficient of NR molecular chains with time during NPT simulation at 298 K and 101 KPa.

S5. The influence of impact velocity on the deformation behavior of polymer chains.

We take the system with 4 nm interlayer distance as an example to investigate the influence of impact velocity on the deformation behavior of polymer chains, and the results are shown in Fig. S5. From Fig. S5(a), the higher the impact velocity, the greater the peak reaction force of the diamond projectile exerted by the nanocomposite substrate. This can be attributed to the increase in yield stress and flow stress with increasing strain rate, which narrows the plastic deformation zone and leads to embrittlement of the substrate. It can be clearly observed from Fig. S5(b) that when the impact velocity of the projectile is up to 10 km/s, brittle fracture occurs in the polymer matrix after the initial linear elastic deformation, which leads to a sudden decrease in non-bond energy dissipation. Meanwhile, when the impact velocity of the projectile is 1 or 2.5 km/s, the potential energy dissipations between polymer chains is almost unchanged, indicating that there is no significant slippage and deformation between the polymer chains. By contrast, when the impact

velocity of the projectile is set to 5 km/s, the polymer matrix has not undergone brittle fracture, and a significant impact-induced potential energy dissipation associated with the non-bond interactions, bond stretching, angle bending can be clearly observed. These results indicate that the impact velocity of 5 km/s is conducive to effective comparative research on the impact resistance of the sample during the impact process. Finally, the morphological snapshots of the nanocomposite substrate after impact at different impact velocities are shown in Fig. S6.

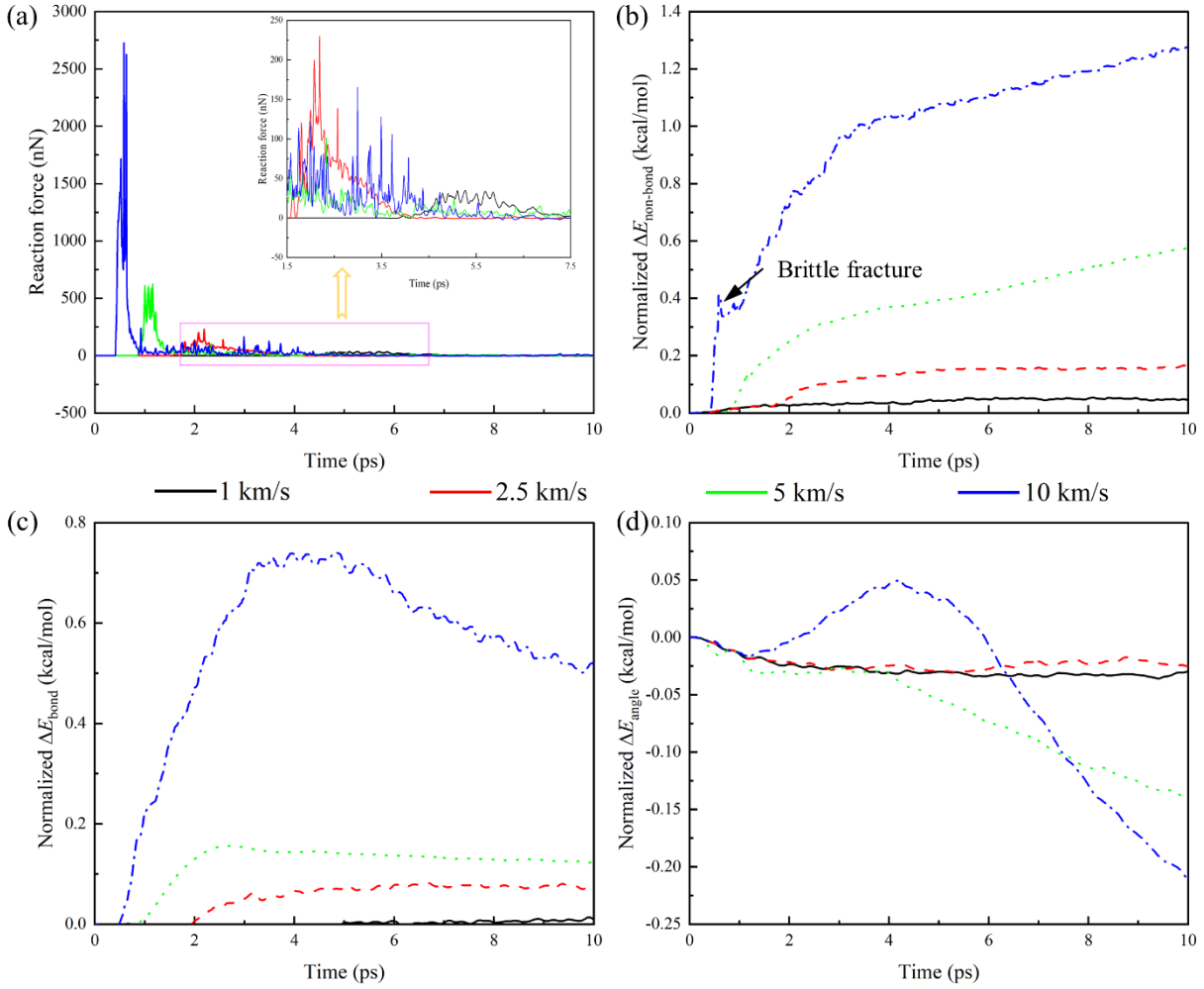

Fig. S5. Variations of (a) the reaction force of the diamond projectile, the dissipations of the potential energies associated with the (b) non-bond interactions, (c) bond stretching, (c) angle bending in the NR matrix with impact velocity.

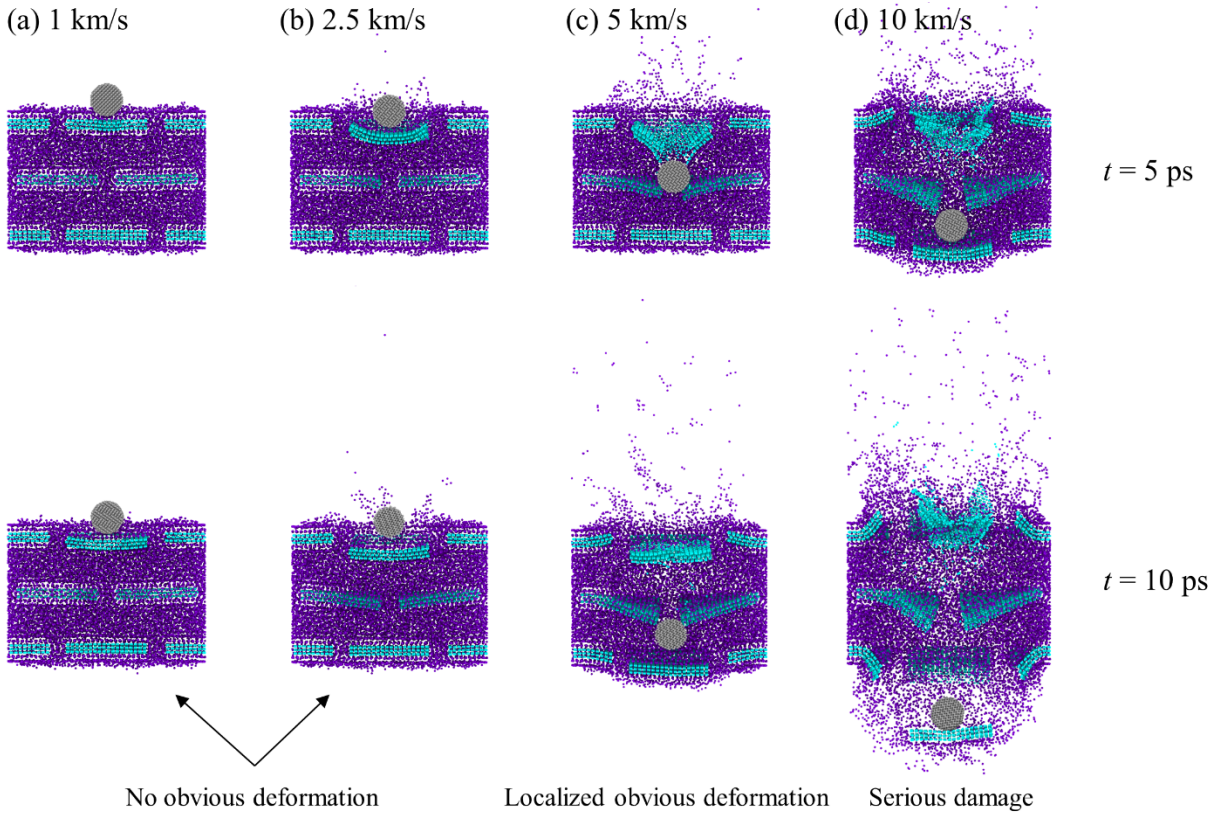

Fig. S6. Morphological snapshots of the nanocomposite substrate after impact at different impact velocities.

S6. Variations of the reaction force and impact velocity of the diamond projectile with time.

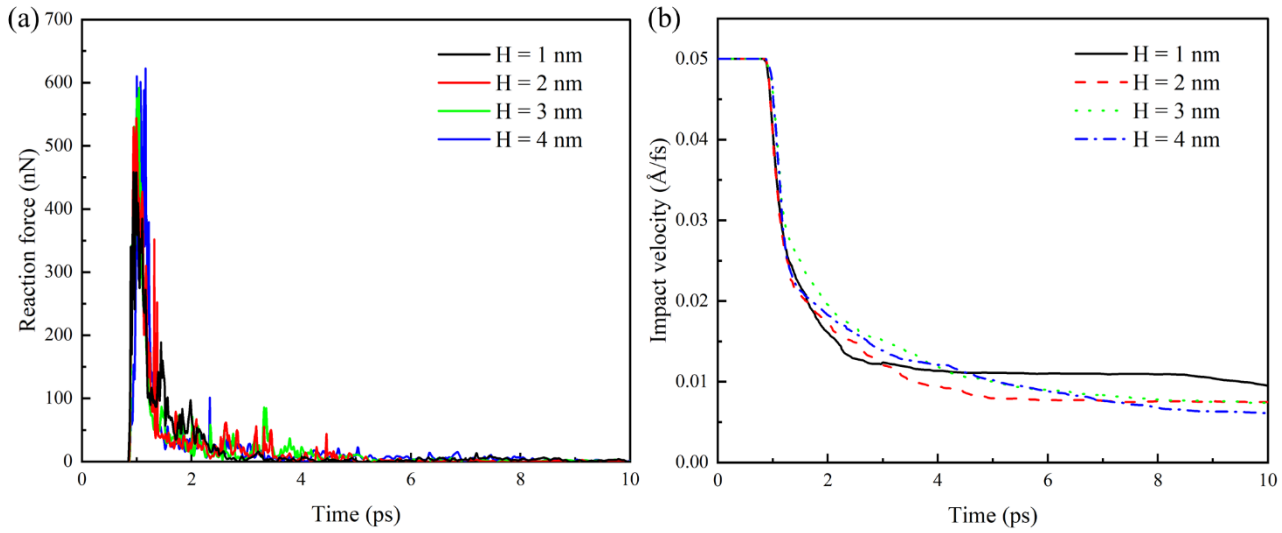

Fig. S7. The variations of the (a) reaction force and (b) impact velocity of the diamond projectile with time at different interlayer distances.

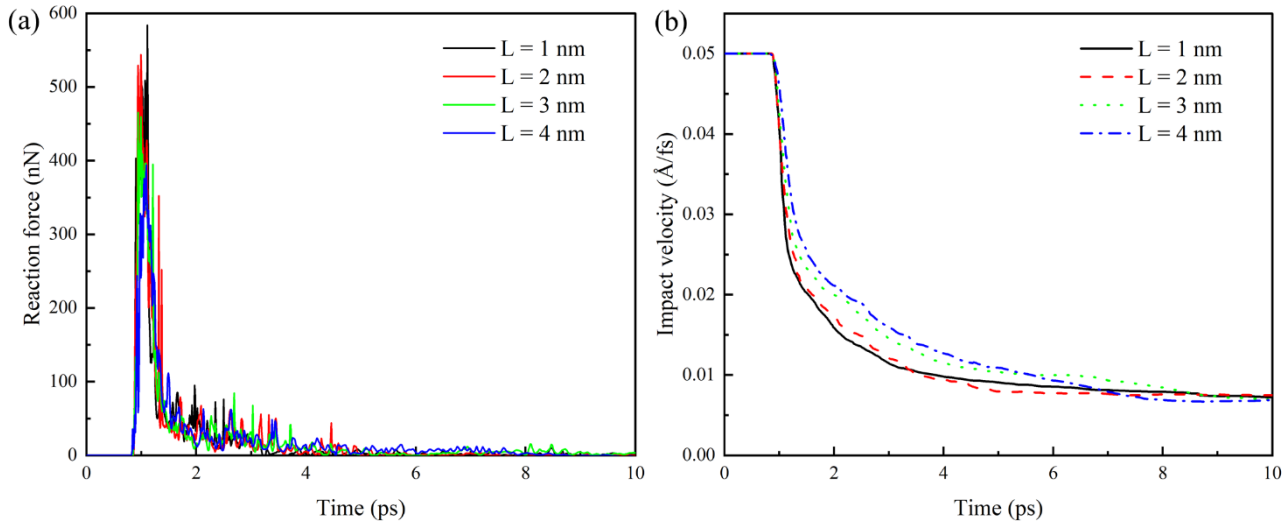

Fig. S8. The variations of the (a) reaction force and (b) impact velocity of the diamond projectile with time at different lateral distances.

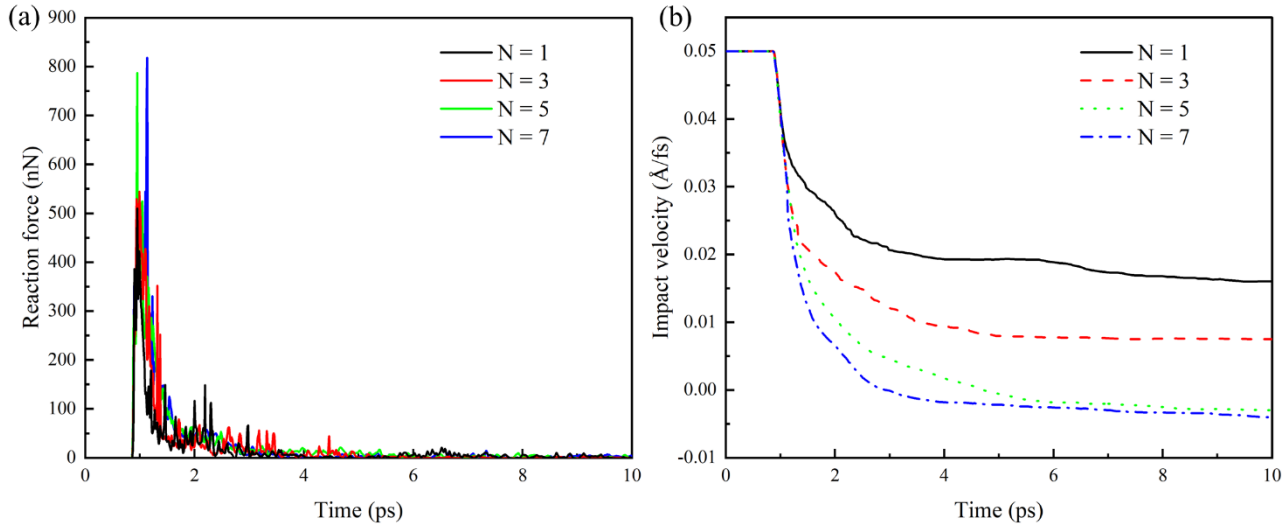

Fig. S9. The variations of the (a) reaction force and (b) impact velocity of the diamond projectile with time at different number of graphene layers.

S7. Variations of the number of broken bonds of polymer chains and graphene layers.

To investigate the effects of geometric parameters of the "brick and mortar" structure on the events of broken bonds of polymer chains and graphene layers, the variations of the number of broken bonds of polymer chains and graphene layers during impact are calculated, respectively, as shown in Fig. S10. As can be seen from Fig. S10, compared to polymer chains, the lower critical bond-breaking length of graphene causes it to break first when struck. From Fig. S10(a) and (d), as the interlayer distance of graphene layers increases, the number of broken bonds in the polymer matrix first significantly increases and then tends to stabilize, while the number of broken bonds in the graphene layers gradually decreases. Based on the theory of micromechanics, the overall

performances of the nanocomposites at the nanoscale are closely related to the characteristics of the matrix, nanofiller, and their interfaces. This can be attributed to the enhanced interfacial interaction and the incompressibility of the polymer matrix, which significantly improves the structural stability and impact resistance of the nanocomposite substrate. Moreover, Fig. S10(b) and (e) show that the number of broken bonds in both the polymer matrix and graphene layers gradually decreases as the lateral distance between graphene layers increases. This result demonstrates that increasing the lateral distance between graphene layers will make graphene more prone to deformation and buffers the diamond projectile through its own deformation and the interfacial interactions with the polymer matrix, leading to a decrease in the number of broken bonds in both the polymer matrix and graphene layers. Finally, Fig. S10(c) and (f) show that as the number of graphene layers increases, the number of broken bonds in the polymer matrix gradually decreases, while the number of broken bonds in the graphene layers first increases significantly and then stabilizes. This result indicates that increasing the number of graphene layers is beneficial to improve the mechanical strength of graphene layers, while also enhancing their interfacial load-transfer behavior with the polymer matrix, allowing more loads to be transferred to the graphene layers and thus resulting in an increase and a decrease in the number of broken bonds in the graphene layer and polymer matrix, respectively.

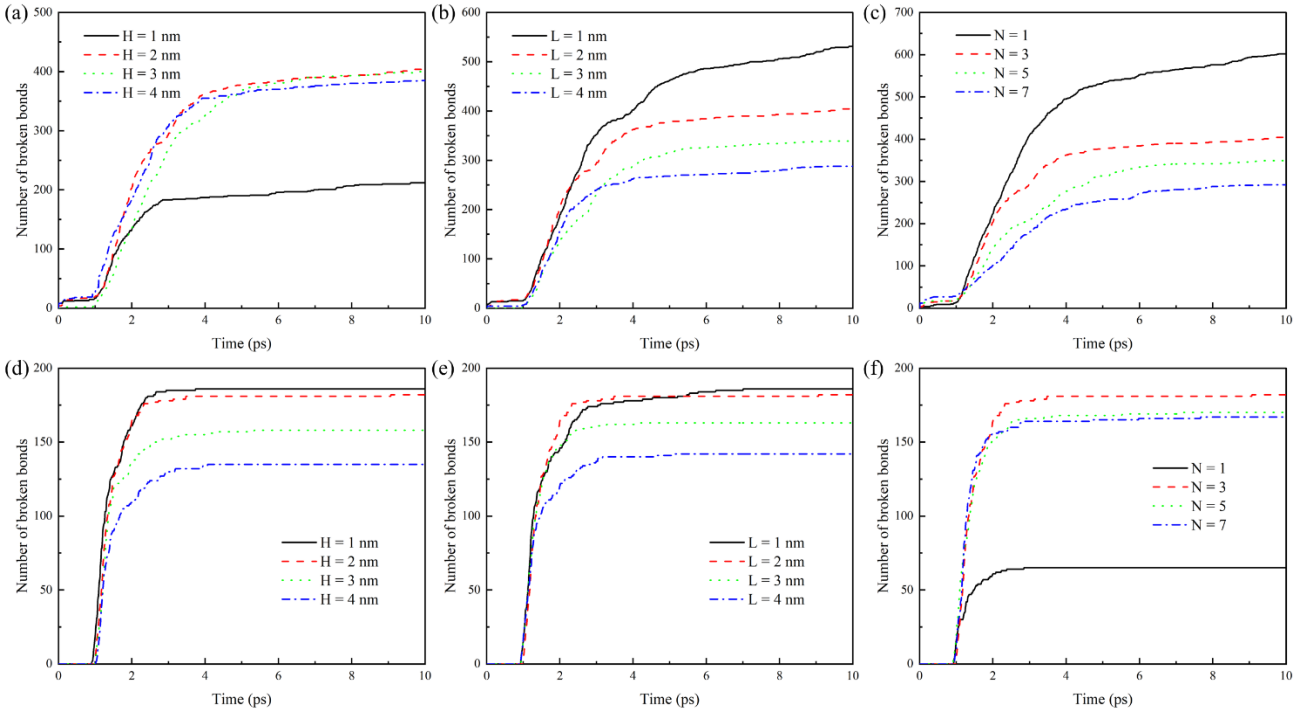

Fig. S10. Variations of the number of broken bonds of (a)-(c) polymer chains and (d)-(f) graphene layers during impact.

S8. The interfacial load-transfer enhancement mechanisms of graphene/polymer nacre-like architecture.

To further investigate the interfacial load-transfer enhancement mechanisms of graphene/polymer nacre-like architecture, the maximum von Mises stresses in the polymer matrix and graphene layers are respectively evaluated by using Equation. (S1). It should be noted that when using OVITO software to calculate von Mises stress, there may be error messages "Could not compute Voronoi cell for some particles" due to the non-periodic boundaries (shrink-wrapped boundary condition) used in the *z* direction, which can be solved by using the Affine Transformation modifier to scale the box size by a factor greater than 1.

$$\sigma_{von} = \sqrt{3\left(\sigma_{xy}^2 + \sigma_{yz}^2 + \sigma_{xz}^2\right) + \frac{1}{2}\left[\left(\sigma_{xx} - \sigma_{yy}\right)^2 + \left(\sigma_{xx} - \sigma_{zz}\right)^2 + \left(\sigma_{zz} - \sigma_{yy}\right)^2\right]} \quad \text{(S1)}$$

where σ_{xx}, σ_{yy}, σ_{zz}, σ_{xy}, σ_{xz}, and σ_{yz} are the virial stress tensor components.

Fig. S11(a) and (b) show the variations of the maximum von Mises stresses in the polymer matrix and graphene layers with time at different interlayer distances, respectively. It can be found that the maximum von Mises stresses in the polymer matrix and graphene layers increase with increasing interlayer distances, indicating an enhanced interfacial load-transfer behavior by improving the interfacial interactions between the polymer matrix and graphene layers.

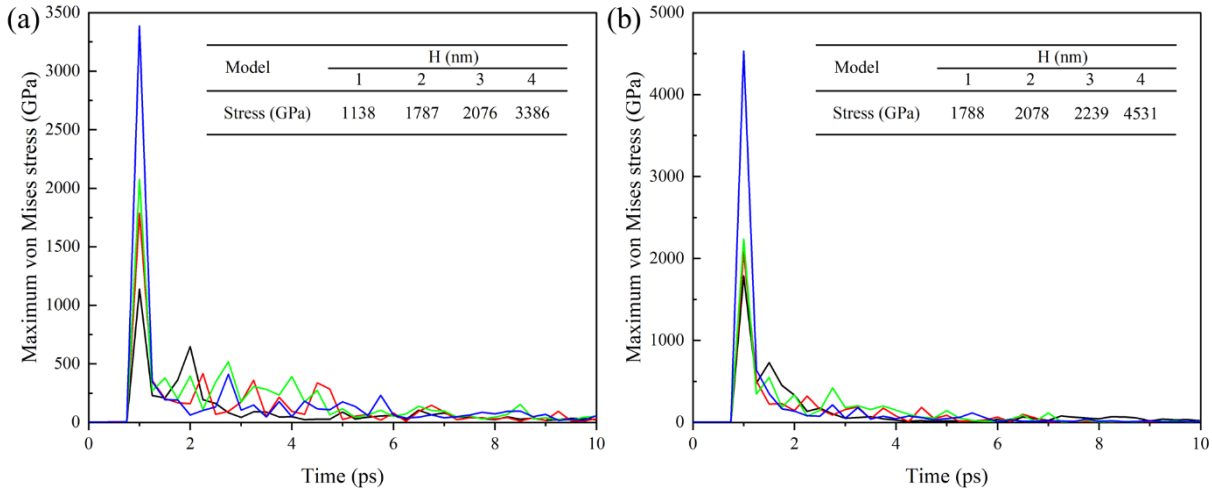

Fig. S11. The variations of the maximum von Mises stress in the (a) polymer matrix and (b) graphene layers with time at different interlayer distances.

Moreover, Fig. S12(a) and (b) show that the as the lateral distance increases, the maximum von Mises stresses in the polymer matrix and graphene layers show a decreasing and slightly increasing trend, respectively. Meanwhile, the increasing effect of graphene layers cannot compensate for the influence of the decreasing effect of the polymer matrix on the overall mechanical properties,

resulting in a decrease in the mechanical properties of the nanocomposites (see Fig. 10).

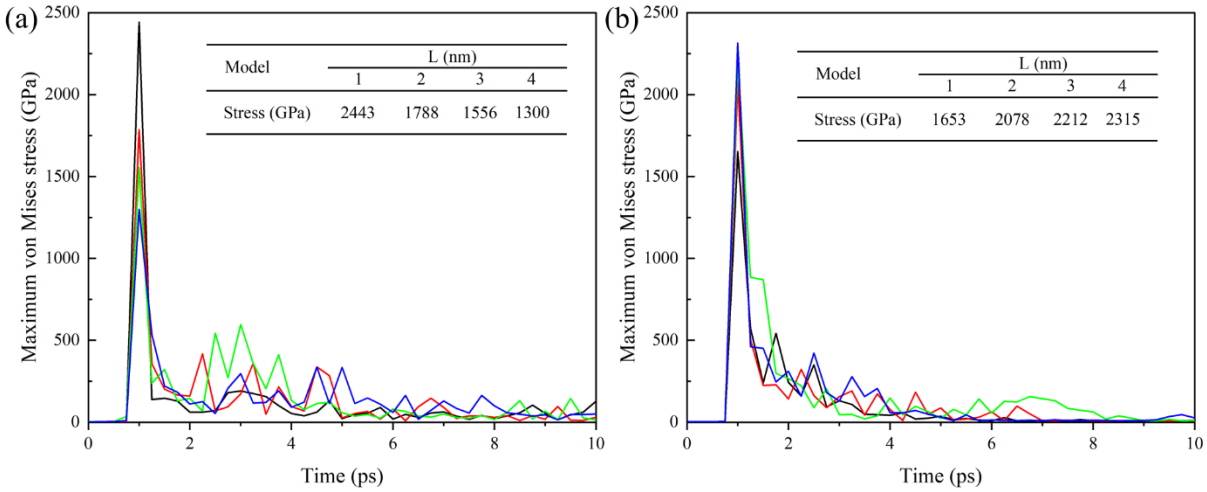

Fig. S12. The variations of the maximum von Mises stress in the (a) polymer matrix and (b) graphene layers with time at different lateral distances.

Furthermore, Fig. S13(a) and (b) show that the as the number of graphene layers increases, the maximum von Mises stresses in the polymer matrix and graphene layers show a decreasing and obviously increasing trend, respectively. This result indicates that the increase in the number of graphene layers enhances the impact resistance of graphene layers, while also enhancing their interfacial load-transfer behavior with the polymer matrix, allowing more loads to be transferred to the graphene layers and resulting in a significant enhancement in the mechanical properties of the nanocomposites (see Fig. 14). Finally, Fig. S14 shows the snapshots of von Mises stress distributions in the nanocomposite substrate at the peak of the maximum von Mises stress curve.

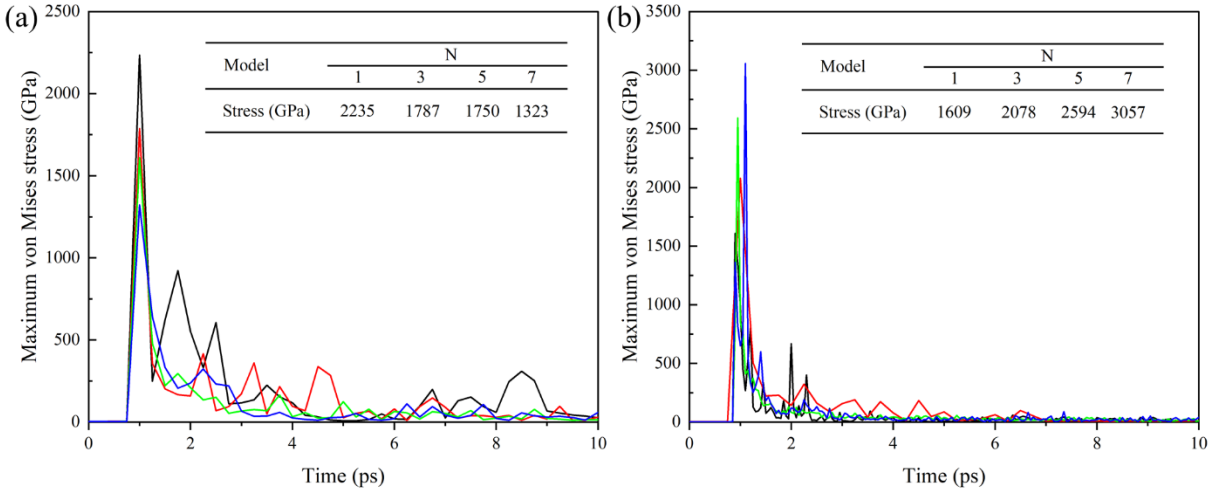

Fig. S13. The variations of the maximum von Mises stress in the (a) polymer matrix and (b) graphene layers with time at different number of graphene layers.

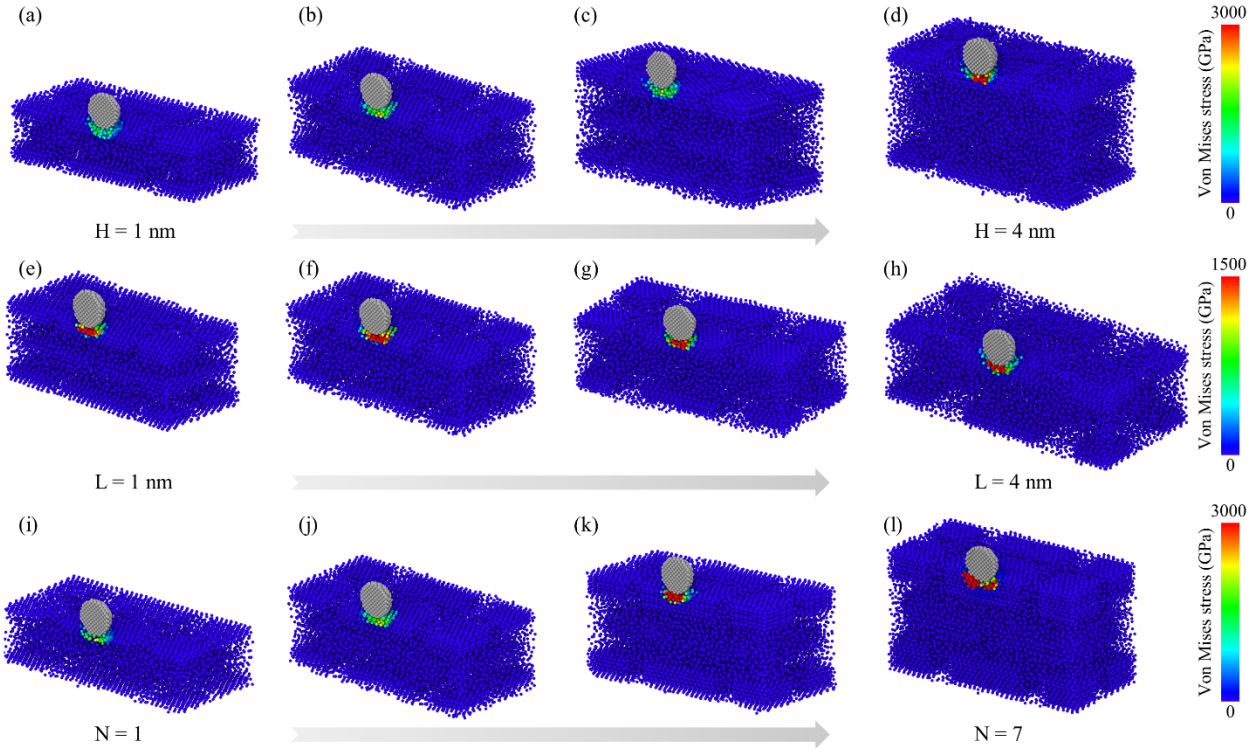

Fig. S14. Snapshots of von Mises stress distributions in the nanocomposite substrate at the peak of the maximum von Mises stress curve (section view).

S9. Effects of graphene lamellar structure on the conformation of rubber molecular chains in a confined environment.

To quantitatively characterize the spatial configuration of rubber molecular chains, the RMS radius of gyration of NR molecular chains is determined, and the results are shown in Fig. S15. From Fig. 15(a)-(c), the RMS radius of gyration of NR molecular chains decreases significantly as the three structural parameters increase, indicating that the lamellar structure of graphene hinders the movement and extension of NR molecular chains. This can be attributed to the enhanced interfacial interactions in confined environment.

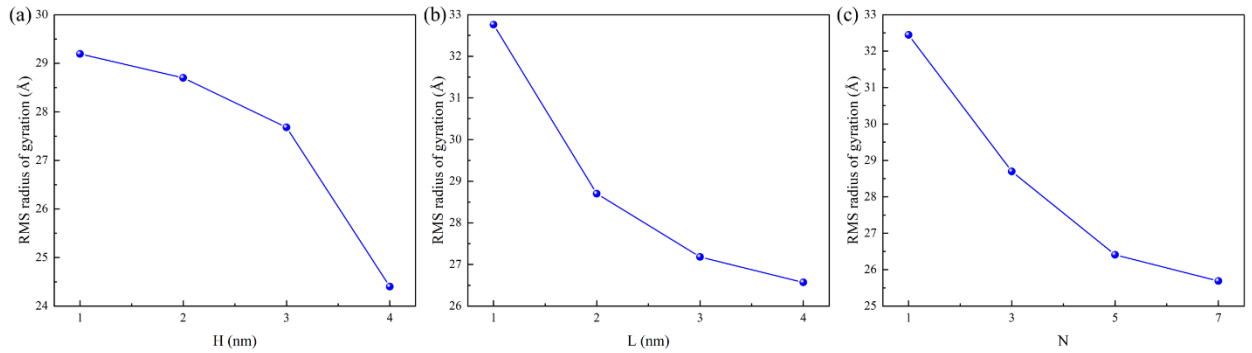

Fig. S15. Effects of the (a) interlayer distance, (b) lateral distance, and (c) number of graphene layers on the RMS radius of gyration of rubber molecular chains.

References

[S1] A.N. Rissanou, V. Harmandaris, Dynamics of various polymer–graphene interfacial systems through atomistic molecular dynamics simulations, Soft Matter, 10 (2014) 2876-2888.